Polymer 51 (2010) 4176–4184

Contents lists available at ScienceDirect

Polymer

journal homepage: www.elsevier.com/locate/polymer

Self-assembly of an A–B diblock copolymer blended with a C homopolymer and a C–D diblock copolymer through hydrogen bonding interaction

Wan-Chun Chen [a], Shiao-Wei Kuo [b,**], Feng-Chih Chang [a,*]

[a] Institute of Applied Chemistry, National Chiao Tung University, Hsin Chu, Taiwan
[b] Department of Materials and Optoelectronic Science, Center for Nanoscience and Nanotechnology, National Sun Yat-Sen University, Kaohsiung, Taiwan

ARTICLE INFO

Article history:
Received 20 December 2009
Received in revised form
2 June 2010
Accepted 4 July 2010
Available online 24 July 2010

Keywords:
Block copolymer
Hydrogen bonding
Self-assembly

ABSTRACT

In this study, we investigated the miscibility, phase behavior, and self-assembled nanostructures formed from the immiscible crystalline-amorphous diblock copolymer poly(ε-caprolactone-*b*-4-vinyl pyridine) (PCL-*b*-P4VP, A–B) when blended with the homopolymer poly(vinyl phenol) (PVPh, C) and the diblock copolymer poly(vinyl phenol-*b*-styrene) (PVPh-*b*-PS, C–D). Long-range-ordered microphase separation was difficult to achieve in the PCL-*b*-P4VP/PVPh (A–B/C) blend system because PVPh interacted with both the P4VP and PCL blocks simultaneously through hydrogen bonding interactions. In contrast, we observed sharp, multiple orders of diffraction in the SAXS profiles of the PCL-*b*-P4VP/PVPh-*b*-PS (A–B/C–D) blend system, indicating that perfect microphase separation occurred because the incorporation of the PS block induced the PVPh block to hydrogen bond preferentially with the P4VP block. This simple A–B/C–D (PCL-*b*-P4VP/PVPh-*b*-PS) diblock copolymer mixture exhibited self-assembly behavior (a three-lamella phase) similar to that of a corresponding ABC triblock copolymer.

1. Introduction

Because diblock copolymers (A-*b*-B) comprising incompatible components can self-assemble into various microphase-separated structures in the bulk state [1–4], they are attractive soft materials for the creation of nanoscale materials exhibiting various functions [5]. Self-assembly of block copolymers plays a key role in the design of new functional supramolecular materials for a wide range of applications such as pollution control and drug delivery. In addition, blends of diblock copolymers and homopolymers often display unusual phase behavior [6–18]. Originally, most studies of diblock copolymer/homopolymer blends concentrated on mixtures of an immiscible A-*b*-B diblock copolymer with an A homopolymer (e.g., a styrenic block copolymer with a polystyrene homopolymer); these systems can exhibit three types of phase behavior (e.g., macro-phase separation, dry-brush, and wet-brush behavior) depending on the molecular weight ratio of the homopolymer A to the block copolymer A [19]. Recently, however, more attention has been placed on the phase behavior of blends of A-*b*-B diblock copolymers and C homopolymers that interact through hydrogen bonding [20–31]. For an A-*b*-B/C blend system, there are four possible outcomes when C is miscible with the A and/or B blocks, as we have discussed in detail previously [31,32].

In addition to diblock copolymer/homopolymer blends, more-complicated macromolecules, such as ABC triblock copolymers, have attracted interest in recent years because they can form more-complicated structures, including three-phase lamellae and core/shell cylinder structures [33]. Although the synthesis of ABC triblock copolymers is complicated, mixing A-*b*-B and C-*b*-D copolymers is a relatively simpler method for preparing such self-assembled morphologies [34,35]. Typically, for such systems, the B and C segments should be attracted through intermolecular interactions (e.g., hydrogen bonding [36–41], electrostatic interactions [42–44], or metal–ligand coordination [45,46]) and the A and D block segments should be incompatible or immiscible. Nevertheless, to the best of our knowledge, very few reports describe the structures of AB/CD blend systems in the bulk state. For example, Mastishita et al. reported that the blending of poly(isoprene-*b*-4-vinyl pyridine) (PI-*b*-P4VP, A-*b*-B) with poly(vinyl phenol-*b*-styrene) (PVPh-*b*-PS, C-*b*-D) formed highly complex hierarchically ordered nanophases, such as lamellae in lamellae structures [34]. In this case, the hydroxyl (OH) groups of PVPh (C) interacted only with the pyridyl groups of P4VP (B) in the PVPh/P4VP complex phase, with the PI (A) with PS (D) segments being

* Corresponding author. Tel./fax: +886 3 5131512.
** Corresponding author. Fax: +886 7 5254099.
E-mail addresses: kuosw@faculty.nsysu.edu.tw (S.-W. Kuo), changfc@mail.nctu.edu.tw (F.-C. Chang).

0032-3861/$ – see front matter © 2010 Elsevier Ltd. All rights reserved.
doi:10.1016/j.polymer.2010.07.006

Table 1
Characterization of PVPh, PVPh-*b*-PS and PCL-*b*-P4VP copolymers.

Copolymer	Repeat unit[a]	M_n[b]	M_w/M_n[b]
PCL-*b*-P4VP(CV)	175–43	24600	1.29
PVPh-*b*-PS(SH)	43–109	16500	1.09
PVPh	–	6100	1.10

[a] Obtained by ^{1}H NMR spectra.
[b] Obtained by GPC trace with DMF or THF eluent of 0.6 ml/min and PS-standard calibration.

immiscible. In this present study, we investigated the effect of changing the nature of the AB/CD diblock copolymers so that the C block would interact with both the A and B blocks through hydrogen bonding, but with the B/C interaction being stronger than the A/C interaction. We expected that such a selective hydrogen bonding interaction would lead to the formation of a variety of composition-dependent microphase-separated structures. We chose to use poly(ε-caprolactone) (PCL) and P4VP as the polymer block species A and B and PVPh and PS as the C and D species in PCL-*b*-P4VP/PVPh-*b*-PS blend systems. In a previous study we found that self-assembled morphology formed from an immiscible PCL-*b*-P4VP diblock copolymer changed in the presence of competitive hydrogen bonding interactions when we increased the PVPh homopolymer content in PCL-*b*-P4VP/PVPh (A-*b*-B/C) blend systems [26]. In this study, we synthesized a PCL-*b*-P4VP diblock copolymer featuring a low molecular weight of P4VP and investigated the differences between the self-assembly behaviors of PCL-*b*-P4VP/PVPh and PCL-*b*-P4VP/PVPh-*b*-PS blend systems.

2. Experimental section

2.1. Materials

ε-Caprolactone (ε-CL, 99.5%, ACROS), 4-vinylpyridine (4-VP, 99.5%, ACROS), styrene (99%, Aldrich), 4-*tert*-butoxystyrene, and toluene (HPLC grade, TEDIA) were distilled from finely ground CaH_2 prior to use. Benzyl peroxide (BPO, >97%) was precipitated from $CHCl_3$ and then recrystallized from MeOH at 0 °C. 4-Hydroxy-2,2,6,6-tetramethylpiperidinyloxy (4-OH-TEMPO, 98%, ACROS), triethylaluminum ($AlEt_3$, 0.9 M in hexane, Fluka), glacial acetic acid (HPLC grade, TEDIA), and *N*,*N*′-dimethylformamide (DMF, HPLC grade, TEDIA) were used without further purification. *sec*-Butyllithium (1.3 M in cyclohexane, ACROS) was used as the initiator for anionic polymerization. Tetrahydrofuran (THF), which was used as polymerization solvent for anionic polymerization, was purified through distillation under Ar from a red THF solution containing diphenylhexyllithium (produced from the reaction of 1,1-diphenylethylene and *n*-butyllithium). Amano Lipase PS was acquired from *Pseudomonas cepacia* and phosphate buffer solution. 0.1 M *N*, *N*′-Methylenebis(acrylamide) (MBA) was obtained from Aldrich Chemical. The detailed synthesis and characterization of the PCL-*b*-P4VP and PVPh-*b*-PS copolymers have been described elsewhere [47–50]. Table 1 and Scheme 1 summarizes the molecular weights and chemical structures of the PVPh homopolymer (H) and PVPh-*b*-PS (SH) and PCL-*b*-P4VP (CV) copolymers employed in this study.

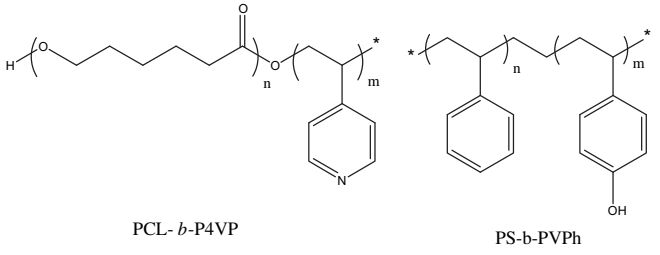

Scheme 1. The chemical structures of block copolymers used in this study.

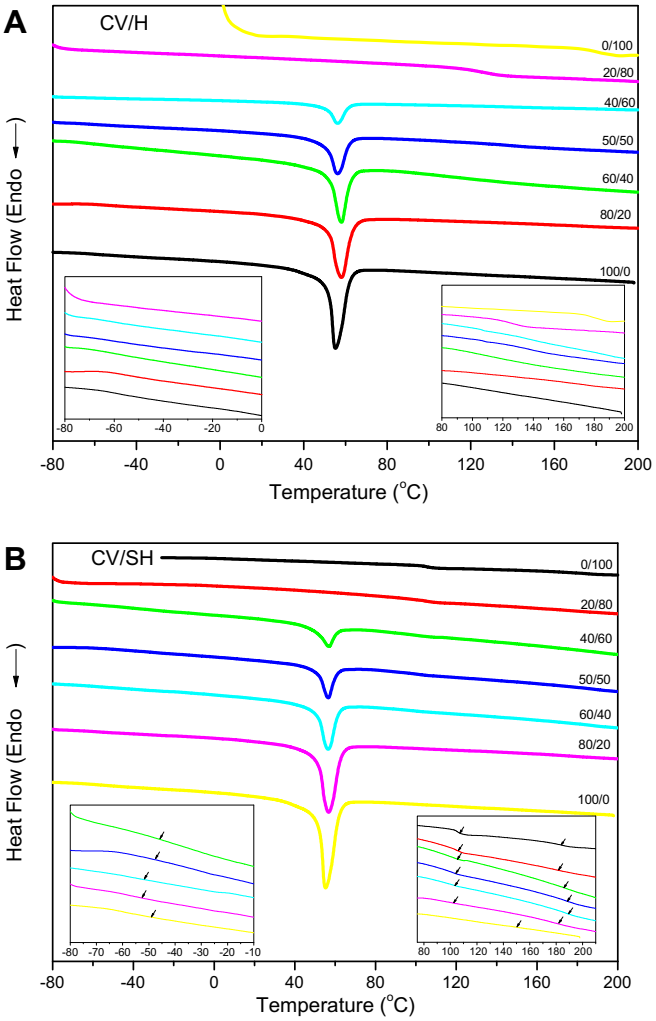

Fig. 1. DSC thermograms of (A) CV/H and (B) CV/SH blends of various compositions.

2.2. Blend preparation

Blended samples of various PCL-*b*-P4VP/PVPh and PCL-*b*-P4VP/PVPh-*b*-PS compositions were prepared through solution-casting.

Table 2
Thermal properties of PCL-*b*-P4VP/PVPh (CV/H) and PCL-*b*-P4VP/PVPh-*b*-PS (CV/HS) blends.

Copolymer	Composition (wt%)	T_f (°C)	T_m (°C)	T_g (°C)
CV/H	100/0	30.2	55.1	−50.3/150.8
	80/20	28.4	58.2	−55.4/172.6
	60/40	28.4	58.0	−56.9/153.2
	50/50	31.3	56.3	−55.7/146.1
	40/60	31.0	56.2	−52.4/137.7
	20/80	–[a]	–	126.5
	0/100	–	–	181.0
CV/HS	100/0	30.2	55.1	−50.3/150.8
	80/20	31.1	56.5	−54.3/101.3/182.1
	60/40	29.7	56.7	−55.1/101.0/188.2
	50/50	30.2	56.5	−49.3/101.2/186.7
	40/60	30.7	56.7	−48.5/101.4/183.2
	20/80	–	–	104.5/179.3
	0/100	–	–	105.9/184.0

[a] It means unobserved T_f and T_m values based on DSC analyses.

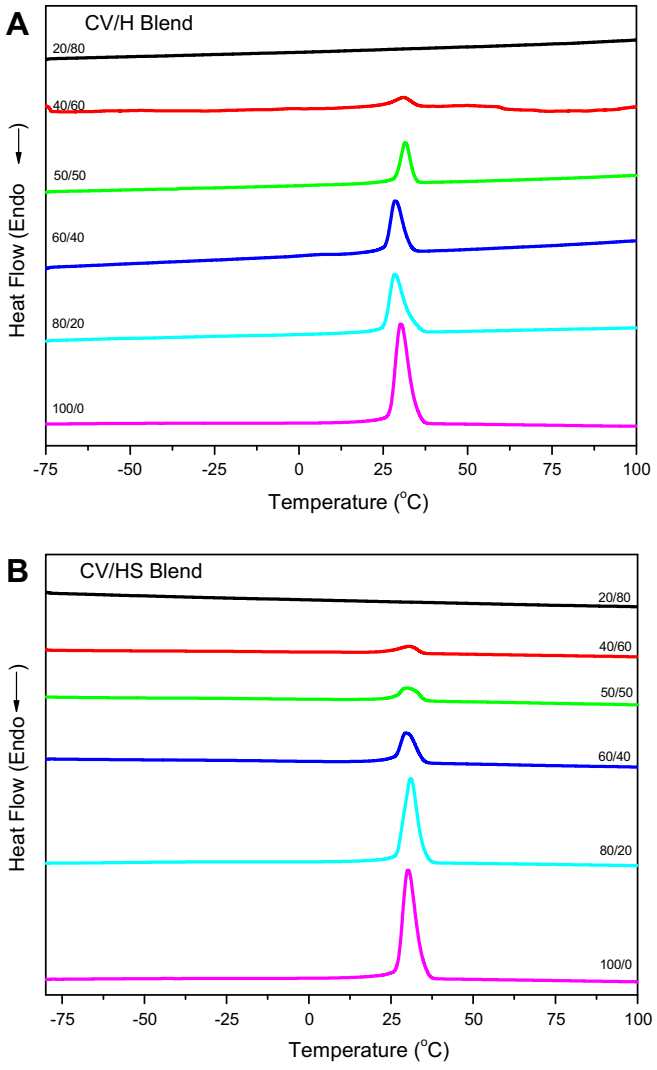

Fig. 2. DSC cooling curves of (A) CV/H blends and (B) CV/HS blends of various compositions.

DMF solutions containing the polymer mixtures (5 wt%) were stirred for 8–10 h and then cast onto a Teflon dish. The solutions were left to evaporate slowly at 80 °C for 1 day and then dried under vacuum at 120 °C for 14 days.

2.3. Characterization

FTIR spectra were measured using a Nicolet Avatar 320 FTIR spectrometer; 32 scans were collected at a resolution of 1 cm^{-1}. The DMF solution containing the sample was cast onto a KBr disk and dried under conditions similar to those used in the bulk preparation. The sample chamber was purged with N_2 and the KBr disk was heated at 120 °C to maintain film dryness. Thermal analysis was performed using a differential scanning calorimeter (DuPont TA Instruments Q-20). The sample (ca. 4–6 mg) was weighed and sealed in an aluminum pan. For non-isothermal crystallization experiments, the samples were first annealed at 210 °C for 10 min and then cooled to −90 °C at a cooling rate of 5 °C/min to record the crystallization exotherm. The temperature corresponding to the exothermic peak is denoted T_f. The glass transition temperature (T_g) was taken as the midpoint of the heat capacity transition between the upper and lower points of deviation from the extrapolated glass and liquid lines, with a scan rate of 20 °C/min over a temperature range from −90 to +250 °C. Transmission electron microscopy (TEM) was performed using a Hitachi H-7100 electron microscope operated at 100 kV. Ultrathin sections of the samples were prepared using a Leica Ultracut S microtome equipped with a diamond knife. Slices of ca. 700 Å thickness were cut at −120 °C. The ultrathin sections were placed onto Cu grids coated with carbon-supporting films, followed by staining through exposure to the vapor from 4% aqueous RuO_4 for 25 min or I_2 for 30 h P4VP, PVPh, PS, and PCL display deep, intermediate, light, and very light contrasts, respectively, when stained with RuO_4 and P4VP exhibits a deep contrast when stained with I_2, thereby enabling the phase behavior in these blend systems to be distinguished. For scanning electron microscopy (SEM) analysis, the samples were coated with Pt and then images were recorded using a Toshiba S4700I emission micrograph operated at a voltage of 5 kV and a beam current of 1×10^{-10} A. Small-angle X-ray scattering (SAXS) experiments were performed using the SAXS instrument at the BL17B3 beam line of the National Synchrotron Radiation Research Center (NSRRC), Taiwan. The blend samples (typical thickness: 1 mm) were sealed between two thin Kapton windows (thickness: 80 μm) and measured at room temperature.

3. Results and discussion

3.1. Thermal analyses

Fig. 1 displays the conventional second-run DSC thermograms (heating rate: 20 °C/min) of the CV/H and CV/HS blends at various compositions. For the PCL-*b*-P4VP block copolymer, we observed two glass transition temperatures (T_g) and a melting temperature (T_m) because of immiscibility between the PCL and P4VP segments. Furthermore, we observed two glass transitions for the PVPh-*b*-PS block copolymer because of immiscibility between the PVPh and PS segments. The values of T_g of the PCL, P4VP, PS, and PVPh block segments were ca. −50, 151, 106, and 181 °C, respectively; the value of T_m of the PCL block was ca. 55 °C, which all amorphous segments are higher than the melting point of PCL crystallites (i.e., hard confinement) [51–54]. Table 2 summarizes the thermal properties of the CV/H and CV/HS blends based on the results of the DSC analyses. The value of T_g of the P4VP block (151 °C) increased and that of the PCL block (−50 °C) remains unchanged for CV/H blends containing 20–40 wt% PVPh (Fig. 1A). Further increasing the PVPh content in the CV/H blend to 50–60 wt% caused the value of T_g of PVPh/P4VP miscible phase to decrease since the hydroxyl group of PVPh tends to interact with the carbonyl group of PCL. Therefore, we speculate that the added PVPh interacted preferentially with the P4VP block through stronger hydrogen bonds; at higher contents, PVPh interacted with both the P4VP and PCL blocks through hydrogen bonding interactions. Meanwhile, CV/H blend has only one glass transition temperature when the PVPh content was 80 wt%, suggesting that the blend had become miscible; i.e., PVPh acted like a common solvent between PCL and P4VP. In contrast, we observed two glass transitions for the corresponding CV/HS blend. Fig. 1B reveals that the value of T_g of the P4VP block increased, while those of the other two blocks (PCL and PS) remained unchanged, for CV/SH blends containing 20–60 wt% PVPh-*b*-PS. Further increasing the PVPh-*b*-PS content in the CV/SH blends to 80 wt% resulted in only two glass transitions—that for the PCL block disappeared, while the values of T_g of the P4VP and PS blocks increased and remained unchanged, respectively. Based on these results, we speculate that incorporating the PS block into the blends induced the PVPh block to form hydrogen bonds more favorably with the P4VP block and decreased its ability to form hydrogen bonds with the PCL block.

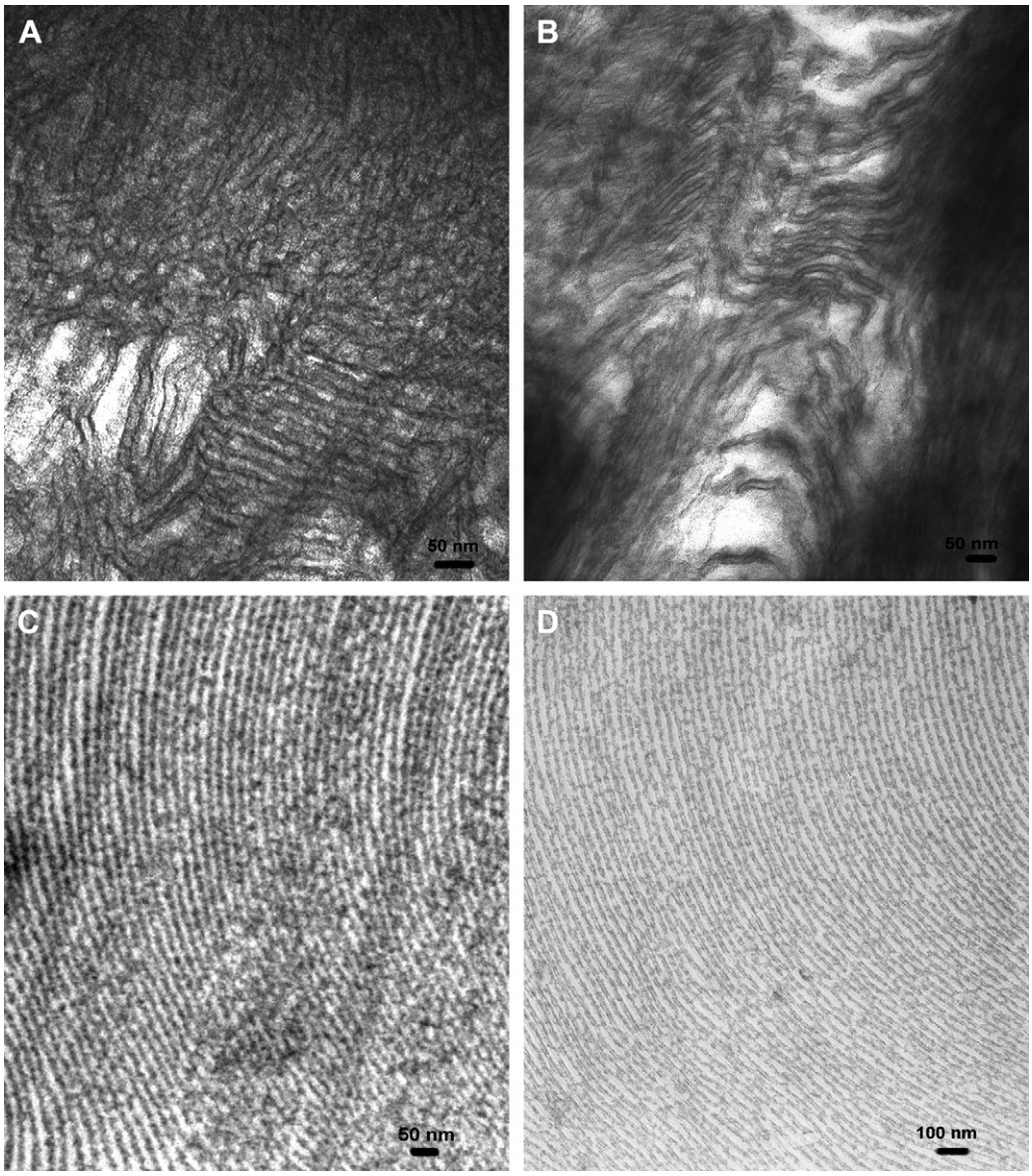

Fig. 3. TEM images of solution-cast films (stained with RuO_4) of the (A) CV/H = 60/40, (B) CV/H = 80/20, (C) CV/SH = 50/50 and (D) CV/SH = 60/40 blends.

Fig. 2 presents DSC cooling curves for the CV/H and CV/HS blends, obtained at a fixed cooling rate of 5 °C/min; Table 2 summarizes the freezing temperatures. The peak temperature of the crystallization exotherm is defined as the freezing temperature (T_f), where a higher value of T_f corresponds to a faster crystallization rate. In general, the freezing temperature (T_f) is associated with non-isothermal crystallization under a fixed cooling rate and displays a distinct correlation with the microdomain structure [55–61]. Chen et al. observed strongly segregated diblock systems under a fixed cooling rate; the freezing temperature associated with non-isothermal crystallization exhibited a distinct correlation with the microdomain structure [55,56]. The degree of supercooling ($\Delta T = T_m^0 - T_f$; $T_m = 75$ °C) required to initiate crystallization in the lamellar microdomains ($\Delta T = 50$ °C) was comparable with that associated with the PCL homopolymer ($\Delta T = 42$ °C) [56]. Fig. 2 reveals that a single exotherm appeared at ca. 28–30 °C for our CV/H blends incorporating 0–60 wt% PVPh and in our CV/SH blends incorporating 0–60 wt% PVPh-*b*-PS; as a result, we would expect lamellar structures in both these blends because their freezing temperatures were almost identical. Notably, however, the difference in the degree of supercooling (ΔT) between the lamellar microdomains of PCL and the PCL homopolymer was too small to confirm the true nanostructures existing in the CV/H and CV/HS blends. Therefore, TEM and SAXS analyses were necessary to elucidate the nanostructures of the CV/H and CV/SH blend systems.

3.2. TEM and SEM analyses

TEM is commonly used to investigate the morphologies of microphase-separated blends. Fig. 3 displays the morphologies of our CV/H and CV/HS blends. Thin films of CV/H and CV/HS blends with various compositions were stained with RuO_4 for 25 min; the P4VP, PVPh, PS and PCL regions provided deep, intermediate, light, and very light contrasts, respectively. Fig. 3A and B reveal that the morphologies of the CV/H = 60/40 and CV/H = 80/20 blends were short-range-ordered lamellar structures, presumably because the low molecular weight of the P4VP segment in the PCL-*b*-P4VP diblock copolymer induced the added PVPh to form hydrogen

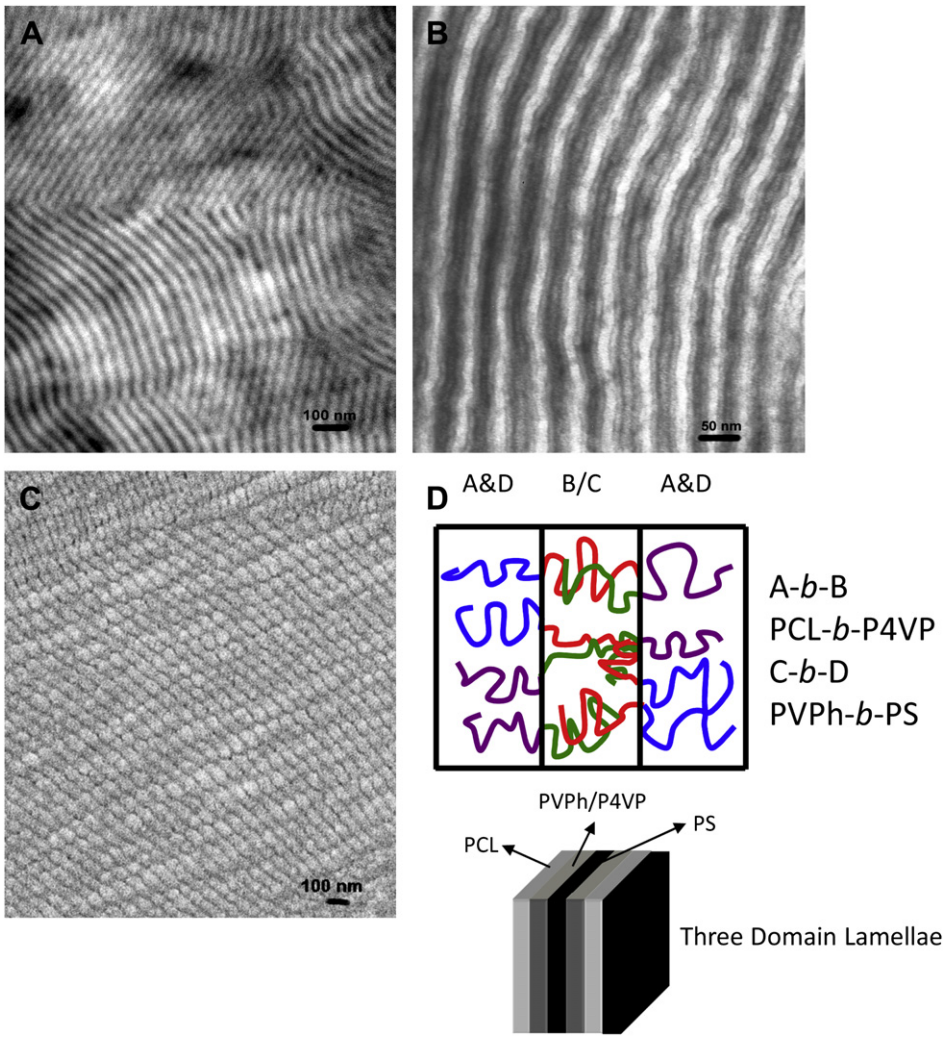

Fig. 4. (A, B) TEM images of solution-cast films of the CV/SH = 80/20 wt% blend stained with (A) I_2 and (B) RuO_4. (C) SEM image of the solution-cast film of the CV/SH = 50/50 blend after degrading the PCL blocks with Lipase PS.

bonds with both the P4VP and PCL blocks. As a result, long-range-ordered nanostructures were difficult to obtain in CV/H blend systems. On the other hand, the morphologies of the CV/HS = 50/50 and CV/HS = 60/40 blends (Fig. 3C and D, respectively) reveal that the CV/HS blends were capable of forming long-range-ordered lamellar structures. We speculate that incorporating the PS block in the blends increased the probability of forming hydrogen bonds between the PVPh and P4VP segments because it acted as an inert diluent segment. In addition, the difference in the solubility parameters of PS [$^{TM}_{PS}$ = 9.04 $(cal/cm^3)^{1/2}$] and PCL [$^{TM}_{PCL}$ = 9.57 $(cal/cm^3)^{1/2}$] also favors the phase separation of PS and PCL [62]. Furthermore, Fig. 4A and B display the morphologies of the CV/HS = 80/20 blend obtained after staining with I_2 and RuO_4, respectively. Because P4VP exhibits a deep contrast upon I_2 staining, it enabled us to distinguish the phase behavior in these blend systems. The dark region in Fig. 4A represents the P4VP/PVPh complex phase; the light region, the excluded (PS + PCL) phase. From comparison with Fig. 4B, we identified a three-lamella structure in the blend stained with RuO_4, with the PS lamella (grey region) located in the middle of the PCL and P4VP/PVPh phases. Moreover, Fig. 4C presents an SEM image of the solution-cast film of CV/HS = 50/50 after degrading the PCL block with Lipase PS for 8 h at 80 °C; the morphology features many lamellar ditches, indicating that the PCL block formed a lamellar structure in the blend, in a good agreement with the TEM image. Note that simple blending of these A–B/C–D diblock copolymers provided morphology (three-phase lamellar structure) similar to those commonly provided by ABC triblock copolymers. In addition, the long-range order in the structure of this A–B/C–D diblock copolymer mixture was superior to that of the corresponding A–B/C diblock copolymer/homopolymer mixture. Fig. 4D shows the possible morphology of this A-*b*-B/C-*b*-D blend system.

Fig. 5 displays the microdomain structures of the CV/H and CV/SH blends of various compositions, as characterized using SAXS. For the CV/H blend system, TEM and SAXS analyses both indicated that microphase separation was controlled by an intricate balance of hydrogen bonding interactions among the three components (PVPh, PCL, and P4VP). The CV/H blends provided broad SAXS peaks, indicating the absence of long-range order in the structure. As we discussed above, the addition of PVPh in this blend system did not lead to perfect microphase separation because the low molecular weight of the P4VP block in the PCL-*b*-P4VP copolymer induced the PVPh homopolymer to form hydrogen bonds with both the P4VP and PCL blocks simultaneously. For this reason, long-range ordering with sharp and multiple scattering peaks was difficultly to obtain in the CV/H blend system, as indicated in Fig. 5A. In contrast, the CV/HS blend system (Fig. 5B) provided a larger degree of long-range ordering and a larger number of sharper scattering peaks relative to

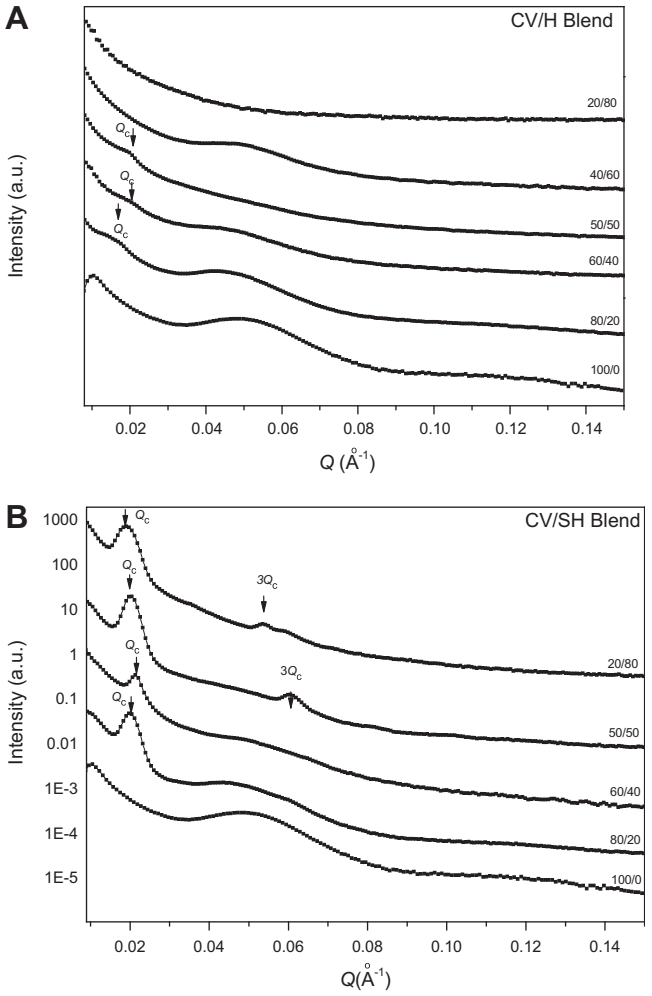

Fig. 5. Profiles of the Lorentz-corrected SAXS intensities, measured at room temperature, of CV/H and CV/SH blends of various compositions.

those of the CV/H blend system. Compositions of CV/HS of 20/80 and 50/50 provided long-range-ordered structures with a ratio of peak positions of 1:3, revealing an ordered phase of lamellae. According to Fig. 5B, the SAXS peaks located at multiple values of Q_c of 0.0184 and 0.0199 $Å^{-1}$ represent lamellar phases having long periods of 34.1 and 31.6 nm, respectively, extracted from the first peak position ($2\pi/Q_c$) for the CV/HS = 20/80 and 50/50 blends, respectively. Combining the TEM and SAXS results, we conclude that long-range order existed in the nanostructures of the CV/HS blends because incorporating the PS block into the blend system increased the probability of hydrogen bonds forming between the PVPh and P4VP segments, thereby favoring microphase separation, which we confirmed through FTIR spectroscopic analyses.

3.3. FTIR spectroscopic analyses

Fig. 6 displays FTIR spectra of various CV/H and CV/HS blends cast from DMF solution at 120 °C (to eliminate the crystal effect of the PCL block and the influence of moisture). Several regions within the FTIR spectra of these blends were influenced by the presence of hydrogen bonding interactions. Pure PVPh revealed (Fig. 6A) two unresolved bands in the region 2700–3800 cm^{-1} (OH stretching region) at 120 °C: one corresponding to the free OH groups at 3525 cm^{-1} and the other, a very broad band centered at 3400 cm^{-1}, to the absorptions of OH groups hydrogen-bonded with other OH groups in the form of dimers and chainlike multimers. The intensity of the signal for the free OH groups decreased gradually upon increasing the PCL-*b*-P4VP content, as expected (cf. Fig. 6A and D). In addition, we know that the PVPh homopolymer forms hydrogen bonds with both the P4VP and PCL blocks, but the strength of the PVPh/P4VP hydrogen bonds was greater than those of the PVPh/PCL blend system. The signals for the OH groups of PVPh and PVPh-*b*-PS shifted to 3125 and 3430 cm^{-1}, respectively, when PCL-*b*-P4VP was present in excess in the blends, indicating that the OH groups interacted preferentially with the pyridyl groups of the P4VP block, with the residual OH groups then interacting with the C=O groups of the PCL block.

The signals for the C=O groups of PCL blocks are sensitive to hydrogen bonding interactions. The peaks at 1735 and 1710 cm^{-1} correspond to the free and hydrogen-bonded C=O groups, respectively. Fig. 6B and E present the C=O stretching regions (1680–1780 cm^{-1}) in the FTIR spectra of the PCL-*b*-P4VP/PVPh and PCL-*b*-P4VP/PVPh-*b*-PS blends, recorded at 120 °C to eliminate the crystal band of PCL at 1724 cm^{-1}. The band for the hydrogen-bonded C=O groups of PCL appeared at 1710 cm^{-1} when PCL-*b*-P4VP was blended with 20 wt% PVPh or 20 wt% PVPh-*b*-PS, indicating that the OH groups of the PVPh segments began to interact with the C=O groups of the PCL block. This phenomenon occurred because of the low fraction of the P4VP block in the PCL-*b*-P4VP copolymer we employed in this study. As expected, a higher content of vinylphenol units resulted in a higher number of hydrogen-bonded C=O groups in both the CV/H and CV/HS blends. In addition, we used the band at 993 cm^{-1} to analyze the hydrogen bonding interactions between the OH groups of PVPh and the pyridyl groups of P4VP. Fig. 6C and F display scale-expanded (980–1020 cm^{-1}) FTIR spectra, recorded at 120 °C, for the CV/H and CV/HS blends. Pure PCL-*b*-P4VP exhibited a characteristic band at 993 cm^{-1} corresponding to the free pyridyl groups in the P4VP blocks. The spectrum of pure PVPh did not feature a signal at 993 cm^{-1}, but rather a band at 1013 cm^{-1}; in the blends, these two bands were well resolved. In the presence of hydrogen bonding between the PVPh and P4VP segments, a new band appeared at 1005 cm^{-1}, which we assigned to the hydrogen-bonded pyridyl units [62]. We employed the Gaussian function to curve-fit the C=O stretching frequencies of PCL at 1735 and 1710 cm^{-1} and the pyridyl bands of P4VP at 993 and 1005 cm^{-1}, corresponding to their respective free and hydrogen-bonded groups. Obtaining the true fraction of hydrogen-bonded groups required knowing the absorptivity ratios for the hydrogen-bonded and free groups; we employed values of α_{HB}/α_F of 1.5 for the C=O groups of PCL and 1.0 for the pyridyl units of P4VP [62,63]. Table 3 summarizes the curve-fitting results for the CV/H and CV/HS blends in terms of the fraction of hydrogen-bonded C=O and pyridyl groups. The PVPh OH groups clearly formed hydrogen bonds with both the P4VP and PCL segments, even when the PVPh content was 20 wt%. In other words, the PVPh OH groups preferentially interacted with the P4VP pyridyl units, with the residual PVPh OH groups then interacting with the PCL C=O groups because of the low content of P4VP in the CV copolymer.

Fig. 7 presents the experimental values for the contents of hydrogen-bonded C=O and pyridyl groups, and the curves predicted using the Painter–Coleman association model [64], with respect to the weight fractions of PVPh in CV/H blends and of PVPh-*b*-PS in CV/HS, determined from the FTIR spectra. Note that the theoretical and experimental data deviated significantly for the contents of PCL hydrogen-bonded C=O groups and P4VP hydrogen-bonded pyridyl groups in the CV/H and CV/HS blend systems. The deviation for the level of PCL hydrogen-bonded C=O groups in the CV/HS blends was smaller than that for the CV/H blends; the situation was reversed for the P4VP hydrogen-bonded

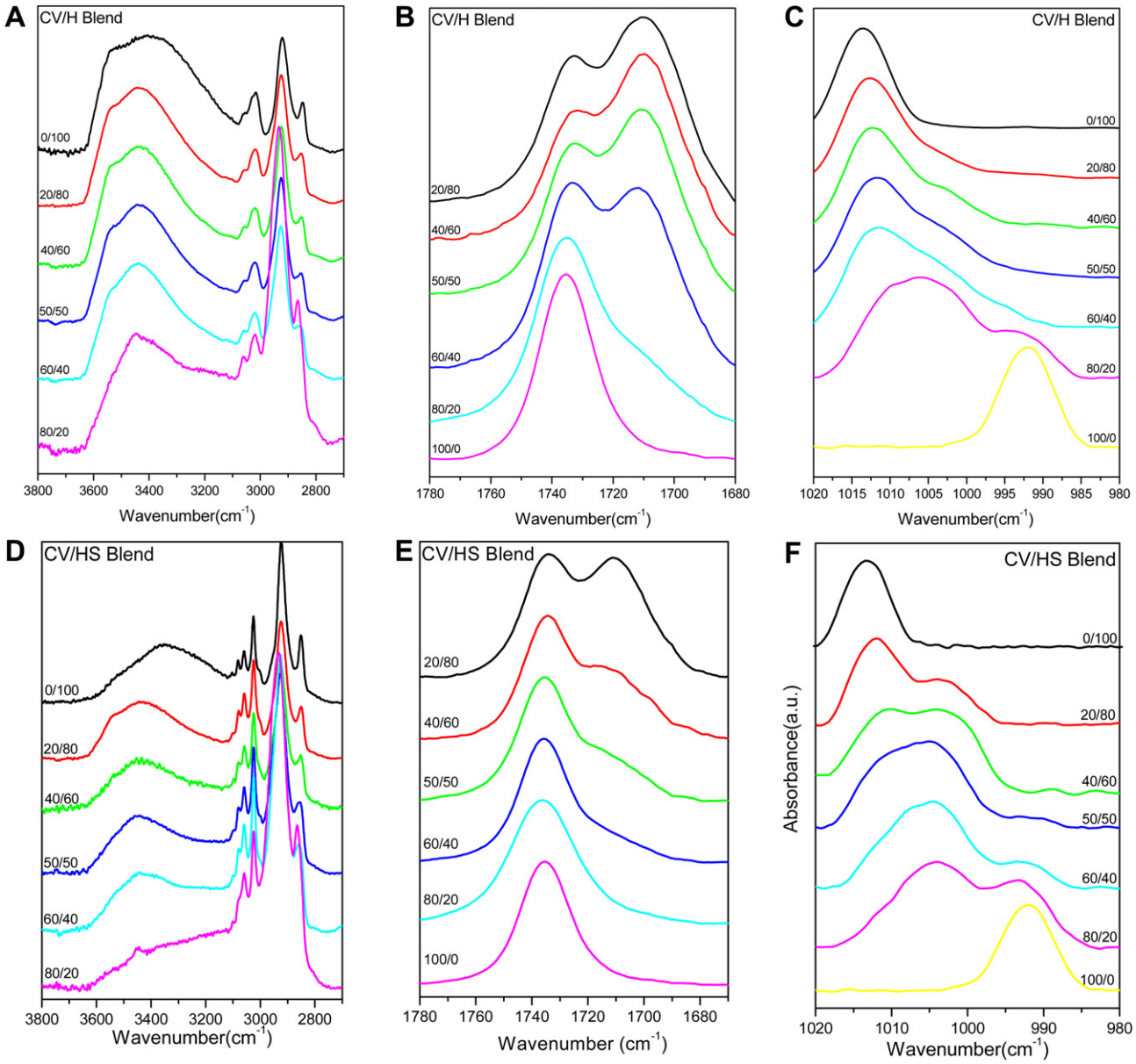

Fig. 6. FTIR spectra, recorded at 120 °C, displaying the (A, D) OH, (B, E) C=O, and (C, F) pyridyl vibration regions for the (A–C) CV/H and (D–F) CV/HS blends.

Table 3
Curving fitting of carbonyl and pyridine groups of CV/H and CV/HS blends.

	ν_f cm^{-1})	A_f (%)	ν_b cm^{-1})	A_b (%)	f_b[a]	ν_f cm^{-1})	A_f (%)	ν_b cm^{-1})	A_b (%)	f_b[a]
CV/H										
100/0	1735	100	–	0	0	992	100	–	0	0
80/20	1734	70.0	1711	30.0	22.2	993	20.4	1005	79.6	79.6
60/40	1735	44.3	1711	55.7	45.6	994	8.5	1004	91.5	91.5
50/50	1735	36.7	1710	63.3	53.4	993	4.9	1004	95.1	95.1
40/60	1735	34.0	1709	66.0	56.4	992	4.8	1004	95.2	95.2
20/80	1734	32.0	1709	68.0	58.7	–	0	1005	100	100
CV/HS										
100/0	1735	100	–	0	0	992	100	–	0	0
80/20	1736	88.6	1712	11.4	7.9	993	34.2	1004	65.8	65.8
60/40	1736	80.4	1711	19.6	14.0	992	15.8	1005	84.2	84.2
50/50	1736	69.4	1711	30.6	22.7	992	6.8	1005	93.2	93.2
40/60	1735	58.2	1711	41.8	32.4	–	0	1003	100	100
20/80	1735	43.4	1710	56.6	46.5	–	0	1004	100	100

[a] f_b: fraction of hydrogen bonding.

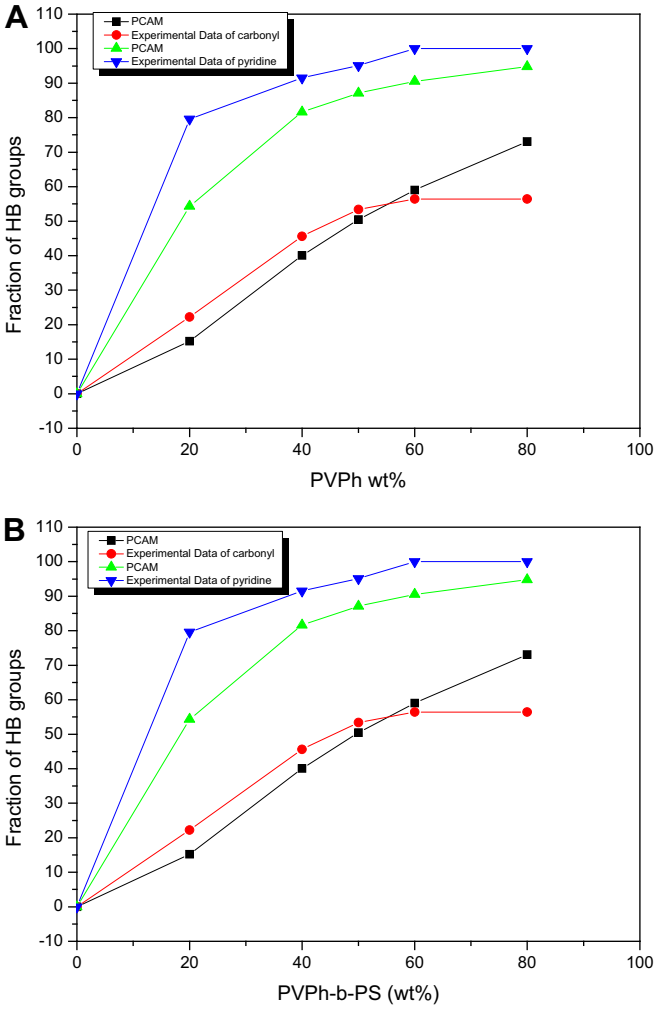

Fig. 7. Experimental and PCAM-predicted data for the contents of hydrogen-bonded C=O and pyridyl units for the (A) CV/H and (B) CV/HS blends.

pyridyl groups. The main reason for these discrepancies in the data obtained for the CV/H and CV/HS blend systems is that the added PS block played an important role as an inert diluent component in the CV/HS blends. In other words, incorporating the PS block increased the probability of forming hydrogen bonds between the PVPh and P4VP segments, due to the incompatibility of the PS block with the other three components and the differences in the strengths of the hydrogen bonds in the PVPh/P4VP and PVPh/PCL interactions.

4. Conclusions

We have used FTIR spectroscopy, DSC, TEM, SEM, and SAXS techniques to investigate the miscibility, phase behavior, and hydrogen bonding interactions in PCL-*b*-P4VP/PVPh and PCL-*b*-P4VP/PVPh-*b*-PS blend systems. FTIR spectra provided evidence that the presence of the PS block increased the probability of hydrogen bonds forming between the PVPh and P4VP segments in the PCL-*b*-P4VP/PVPh-*b*-PS blend system, due to incompatibility of the PS block with the other three components and the differences in the strengths of the hydrogen bonds in the PVPh/P4VP and PVPh/PCL interactions. Moreover, DSC analysis revealed that incorporating the PS block into the blends induced the PVPh block to form hydrogen bonds more favorably with the P4VP block and less favorably with the PCL block. TEM and SEM images and SAXS analysis indicated that more-perfect microphase separation occurred in the PCL-*b*-P4VP/PVPh-*b*-PS blend system than in the PCL-*b*-P4VP/PVPh blend system. We conclude that the main reason for the different degrees of microphase separation in the PCL-*b*-P4VP/PVPh and PCL-*b*-P4VP/PVPh-*b*-PS blend systems was the incompatibility of the PS block with the other three components; this phenomenon increased the probability of hydrogen bonds forming between the PVPh and P4VP segments.

Acknowledgment

This work was supported financially by the National Science Council of the R.O.C. under Contract No. NSC 97-2221-E-110-013-MY3 and NSC 98-2221-E-110-006.

References

[1] Matsuo M, Ueno T, Horino H, Chujyo S, Asai H. Polymer 1968;9:425.
[2] Helfand E, Tagami Y. J Chem Phys 1972;56:3592.
[3] Lodge TP. Macromol Chem Phys 2003;204:265.
[4] Ruzatte AV, Leibler L. Nat Mater 2005;4:19.
[5] Forster S, Plantenberg T. Angew Chem Int Ed 2002;41:688.
[6] Han YK, Pearce EM, Kwei TK. Macromolecules 2000;33:1321.
[7] Zhao JQ, Pearce EM, Kwei TK. Macromolecules 1997;30:7119.
[8] Bendejacq D, Ponsinet V, Joanicot M. Macromolecules 2002;35:6645.
[9] Zoelen WV, Ekenstein GA, Ikkala O, ten-Brinke G. Macromolecules 2006;39:574.
[10] Huang P, Zhu L, Cheng SZD, Ge Q, Quirk RP, Thomas EL, et al. Macromolecules 2001;34:649.
[11] Jinnai H, Hasegawa H, Nishikawa Y, Sevink GJ, Braunfeld MB, Agard DA, et al. Macromol Rapid Commun 2006;27:1424.
[12] Tucker PS, Paul DR. Macromolecules 1988;21:2801.
[13] Hashimoto T, Tanaka H, Hasegawa H. Macromolecules 1990;23:4378.
[14] Jiang M, Xie HK. Prog Polym Sci 1991;16:977.
[15] Jiang M, Huang T, Xie J. Macromol Chem Phys 1995;196:787.
[16] Jiang M, Huang T, Xie J. Macromol Chem Phys 1995;196:803.
[17] Vavasour JD, Whitmore MD. Macromolecules 2001;34:3471.
[18] Maurer WW, Bates FS, Lodge TP. J Chem Phys 1998;108:2989.
[19] Koizumi S, Hasegawa H, Hashimoto T. Macromolecules 1994;27:7893.
[20] Bosse AW, Tirumala VR, Lin EK. J Polym Sci Part B Polym Phys 2009;47:2083.
[21] Hameed N, Guo Q. Polymer 2008;49:922.
[22] Hameed N, Guo Q. Macromolecules 2008;41:7596.
[23] Hameed N, Guo Q. Polymer 2008;49:5268.
[24] Chen WC, Kuo SW, Lu CH, Chang FC. Macromolecules 2009;42:3580.
[25] Lee HF, Kuo SW, Huang CF, Lu JS, Chan SC, Chang FC. Macromolecules 2006;39:5458.
[26] Chen WC, Kuo SW, Jeng US, Chang FC. Macromolecules 2008;41:1401.
[27] Dobrosielska K, Wakao S, Takano A, Matsushita Y. Macromolecules 2008;41:7695.
[28] Zhou J, Shi AC. J Chem Phys 2009;130:234904.
[29] Dobrosielska K, Wakao S, Suzuki J, Noda K, Takano A, Matsushita Y. Macromolecules 2009;42:7098.
[30] Lin IH, Kuo SW, Chang FC. Polymer 2009;50:5276.
[31] Chen SC, Kuo SW, Jeng US, Chang FC. Macromolecules 2010;43:1083.
[32] Kuo SW. Polym Inter 2009;58:455.
[33] Rodriguez-Hernandez J, Checot F, Gnanou Y, Lecommandoux S. Prog Polym Sci 2005;30:691.
[34] Matsushita Y. Macromolecules 2007;40:771.
[35] Matsushita Y, Takano A, Hayashida K, Asari T, Noro A. Polymer 2009;50:2191.
[36] Li G, Shi L, Ma R, An Y, Huang N. Angew Chem Int Ed 2006;45:4959.
[37] Kuo SW, Tung PH, Lai CL, Jeong KU, Chang FC. Macro Rapid Commun 2008;29:223.
[38] Hsu CH, Kuo SW, Chen JK, Ko FH, Liao CS, Chang FC. Langmuir 2008;24:7727.
[39] Kuo SW, Tung PH, Chang FC. Eur Polym J 2009;45:1924.
[40] Liu X, Jiang M, Yang S, Chen M, Chen D, Yang C, et al. Angew Chem Int Ed 2002;41:29503.
[41] Yan X, Liu G, Hu J, Willson CG. Macromolecules 2006;39:1906.
[42] Gohy JF, Varshney SK, Jerome R. Macromolecules 2001;34:3361.
[43] Harada A, Kataoka K. Science 1999;283:65.
[44] Fukushima S, Miyata K, Nishiyama N, Kanayama N, Yamasaki Y, Kataoka K. J Am Chem Soc 2005;127:2810.
[45] Gohy JF, Hofmeier H, Alexeev A, Schubert US. Macromol Chem Phys 2003;204:1524.
[46] Zhang GZ, Liu S, Zhao H, Jiang M. Mater Sci Eng C 1999;10:155.
[47] Lin CL, Chen WC, Liao CS, Su YC, Huang CF, Kuo SW, et al. Macromolecules 2005;38:6435.
[48] Lu CH, Huang CF, Kuo SW, Chang FC. Macromolecules 2009;42:1067.
[49] Tung PH, Kuo SW, Chang FC. Polymer 2007;48:3192.
[50] Chan SC, Kuo SW, Lu CH, Lee HF, Chang FC. Polymer 2007;48:5059.
[51] Huang P, Zhu L, Gau Y, Ge Q, Jing AJ, Chen WY, et al. Macromolecules 2004;37:3689.
[52] Zhu L, Cheng SZD, Callhoun BH, Ge Q, Quirk RP, Thomas EL, et al. Macromolecules 2001;34:1244.

[53] Zhu L, Cheng SZD, Calhoun BH, Ge Q, Quirk RP, Thomas EL, et al. J Am Chem Soc 2000;122:5957.
[54] Zhu L, Cheng SZD, Hunag P, Ge Q, Quirk RP, Thomas EL, et al. Adv Mater 2002;14:31.
[55] Chen HL, Hsiao SC, Lin TL, Yamauchi K, Hasegawa H, Hashimoto T. Macromolecules 2001;34:671.
[56] Chen HL, Wu JC, Lin TL, Lin JS. Macromolecules 2001;34:6936.
[57] Loo YL, Register RA, Ryan AJ, Dee GT. Macromolecules 2001;34:8968.
[58] Chen HL, Lin SY, Huang YY, Chiu FC, Liou W, Lin JS. Macromolecules 2002; 35:9434.
[59] Xu JT, Turners SC, Fairclough JPA, Mai SM, Ryan AJ, Chaibundit C, et al. Macromolecules 2002;35:3614.
[60] Hsu JY, Hsieh IF, Nandan B, Chiu FC, Chen JH, Jeng US, et al. Macromolecules 2007;40:5014.
[61] He CL, Sun JR, Deng MX, Chen XS, Jing XB. Biomacromolecules 2004;5:2042.
[62] Coleman MM, Graf JF, Painter PC. Specific interactions and the miscibility of polymer blends. Lancaster, PA: Technomic Publishing; 1991.
[63] Cesteros LC, Meauiro E, Katime I. Macromolecules 1993;26:2323.
[64] Coleman MM, Painter PC. Miscible polymer blend-background and guide for calculations and design. Destech Publications, Inc.; 2006.